DNA Hydrolysis and Oxidative Cleavage by Metal-Binding Peptides Tethered to Rhodium Intercalators†

Kimberly D. Copeland, Marilena P. Fitzsimons,‡ Robert P. Houser,§ and Jacqueline K. Barton*

Division of Chemistry and Chemical Engineering, California Institute of Technology, Pasadena, California 91125

Received September 14, 2001; Revised Manuscript Received November 2, 2001

ABSTRACT: With the goal of developing artificial nucleases for DNA hydrolysis, metal-coordinating peptides have been tethered to a DNA-intercalating rhodium complex to deliver metal ions to the sugar−phosphate backbone. The intercalator, $[Rh(phi)_2bpy']Cl_3$ [phi = 9,10-phenanthrenequinone diimine; bpy′ = 4-(butyric acid)-4′-methyl-2,2′-bipyridine], provides DNA binding affinity, and a metal-binding peptide contributes reactivity. This strategy for DNA hydrolysis is a general one, and zinc(II)-promoted cleavage has been demonstrated for two widely different tethered metallopeptides. An intercalator coupled with a de novo-designed α helix containing two histidine residues has been demonstrated to cleave both supercoiled plasmid and linear DNA substrates. Mutation of this peptide confirms that the two histidine residues are essential for Zn^{2+} binding and cleavage. Zinc(II)-promoted cleavage of supercoiled plasmid has also been demonstrated with an intercalator−peptide conjugate containing acidic residues and modeled after the active site of the *Bam*HI endonuclease. Other redox-active metals, such as copper, have been delivered to DNA with our intercalator−peptide conjugates to effect oxidative chemistry. Copper cleavage experiments and photocleavage experiments with $[Rh(phi)_2bpy']^{3+}$ complement the hydrolysis studies and provide structural information about the interactions between the tethered metallopeptides and DNA. Variation of the rhodium intercalator was also explored, but with a mismatch-specific intercalator, no site-specific hydrolysis was found. These experiments, in which the peptide, the metal cation, and the intercalator components of the conjugate are each varied, illustrate some of the issues involved in creating an artificial nuclease with DNA intercalators and metallopeptides.

The phosphodiester bonds of DNA are remarkably resistant to hydrolysis under physiological conditions (*1*−*3*). By recruiting metal cofactors and forming extensive contacts with the nucleic acid substrate, nucleases are able to accelerate the phosphodiester hydrolysis reaction by factors as great as 10^{16}, and thus make possible the manipulations of DNA that are essential for life (*4*). Although many of these enzymes have been harnessed for use in the laboratory, there is a great deal of interest in the design of artificial nucleases, small molecular scissors that can bind at a specific sequence of interest and cleave DNA hydrolytically. Such reagents would eliminate many of the potential problems (instability, stringent conditions, etc.) associated with the larger, natural DNA-binding enzymes, and would have wide applicability as tools in molecular biology or as probes of the structure and function of nucleic acids. Additionally, well-characterized small molecules may provide insight into the roles metals play in natural hydrolases (*5*). Although small molecules that cleave DNA by oxidative mechanisms are useful for many applications (*6*−*8*), they are not suited to all applications and they do not contribute to our understanding of natural hydrolases. In contrast to hydrolytic agents, oxidative agents form products that are incompatible with enzymatic manipulation. In addition, some oxidative molecules create diffusible oxygen species and thus cause indiscriminate damage to DNA.

A handful of promising small molecules have been reported to cleave DNA hydrolytically (*9*). Almost all of these artificial nucleases rely on transition metals or lanthanide metals for hydrolysis of the DNA backbone. Stable Co(III) complexes have been demonstrated to promote DNA hydrolysis through both Lewis acid activation of the phosphate and nucleophilic attack of a coordinated hydroxide (*10*, *11*). A variety of Cu(II) complexes have also been used for DNA hydrolysis (*12*−*14*). However, many of these complexes can also oxidize DNA in the presence of reducing agents, and this complicates both analysis and application. Complexes with Zn(II) are particularly interesting because this metal center is not redox-active, but only a few artificial nucleases boasting Zn(II) have been demonstrated to cleave DNA (*15*, *16*). Though lanthanides provide impressive acceleration of DNA hydrolysis (*17*−*19*), they are generally difficult to solubilize and characterize. Cerium, because it can be oxidized to Ce^{4+}, is one of the most effective lanthanide metals for DNA hydrolysis (*20*, *21*). Above pH 4, Ce^{4+} actually forms a hydroxide gel; although efficient, this turbid

† This work was supported by the NIH (Grant GM33309). The NIH also provided NRSA predoctoral (K.D.C.) and postdoctoral (R.P.H.) fellowships, and NSERC provided a predoctoral fellowship (M.P.F.).

* To whom correspondence should be addressed. E-mail: jkbarton@its.caltech.edu.

‡ Present address: Department of Chemistry, Stonehill College, Easton, MA 02357.

§ Present address: Department of Chemistry and Biochemistry, University of Oklahoma, Norman, OK 73019.

10.1021/bi011793k CCC: $22.00
Published on Web 12/11/2001

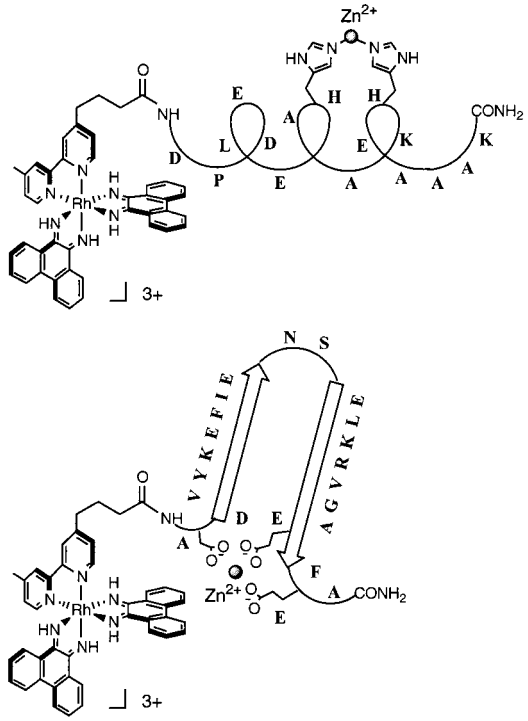

FIGURE 1: Schematic illustration of intercalator−peptide conjugates: (top) $[Rh(phi)_2bpy'\text{-}P1]^{3+}$ and (bottom) $[Rh(phi)_2bpy'\text{-}Bam]^{3+}$. The conjugates combine DNA-binding and reactive moieties; the rhodium intercalator binds in the major groove with high affinity, and the tethered peptide binds divalent cations to promote reaction at the DNA backbone.

system is not practical for many applications. Efforts are currently focused on the development of ligands that solubilize Ce^{4+} without reducing activity (*22*).

Model studies with crystallographically characterized dinuclear metal complexes emphasize the advantages of placing two metal centers together for cooperative activation of a substrate (*1*), and a number of laboratories have created ligands that incorporate two metals. Most recently, a novel dicerium complex that cleaves both plasmid and linear DNA was reported (*23*). Notably, plasmid cleavage experiments suggest that the complex cleaves DNA by double-strand cutting.

The artificial nucleases reported to date typically provide rate enhancements on the order of 10^6-10^7. Cu^{2+} complexes of kanamycin and neamine were reported to cleave DNA under hydrolytic conditions with a >1 million-fold rate enhancement, and this represents the most significant acceleration observed to date (*24*). Although significant strides have clearly been made toward the design of artificial nucleases for DNA hydrolysis, we are still far from creating practical laboratory tools.

Our strategy for the development of artificial synthetic nucleases involves harnessing a rhodium intercalator for delivery of short metallopeptides to the DNA backbone. We previously reported the hydrolysis of plasmid DNA and oligonucleotide substrates with a zinc-binding peptide (P1 = Asp-Pro-Asp-Glu-Leu-Glu-His-Ala-Ala-Lys-His-Glu-Ala-Ala-Ala-Lys-$CONH_2$) tethered to a DNA−intercalating rhodium complex (Figure 1) (*25*). Our conjugate has three important components: (i) a designed peptide with residues for metal coordination, (ii) a divalent cation delivered to the sugar−phosphate backbone, and (iii) a DNA-binding moiety.

The DNA-binding portion of the Rh−P1 conjugate, $[Rh(phi)_2bpy]^{3+}$,[1] is known to intercalate with high affinity from the major groove ($K_B > 10^7\ M^{-1}$), and upon photoactivation to cleave DNA at the binding site (*26*, *27*). The photocleavage reaction occurs upon irradiation of the metal complex at 313 nm, and proceeds through abstraction of a hydrogen atom from the ribose ring and subsequent strand scission (*27*). This oxidative cleavage of the DNA reveals the binding sites of the intercalator, and is a very convenient property as we seek to design metallointercalator conjugates for DNA hydrolysis. The photocleavage pattern observed for $[Rh(phi)_2bpy]^{3+}$ suggests sequence neutral binding, with only a slight preference for 5′-Pu-Py-Pu-Py-3′ sites (*28*).

The reactive peptide of the Rh−P1 conjugate was designed de novo to be α helical and to contain histidine residues for Zn^{2+} coordination. In the presence of Zn^{2+}, micromolar concentrations of the conjugate converted supercoiled (I) pBR322 DNA to nicked (II) and linear (III) forms with a pseudo-first-order rate constant of $(2.5 \pm 0.2) \times 10^{-5}\ s^{-1}$ for the disappearance of supercoiled plasmid (*25*). Although the helicity of the peptide is modest (20−25%), it is interesting that both helical content and cleavage activity reach a maximum at stoichiometric amounts of Zn^{2+}. By high-resolution polyacrylamide gel electrophoresis, the products of an oligonucleotide cleavage reaction with the Rh−P1 conjugate were found to contain 3′-hydroxyl and not 3′-phosphate termini (*25*). Together, these results suggest that stereospecific hydrolysis of both plasmid and linear DNA can be accomplished under mild conditions with low concentrations of the intercalator−peptide complex.

Here we describe efforts to explore and optimize each component of the Rh−P1 conjugate. The composition of P1 has been mutated; the system has been tested with a variety of redox-active and -inactive metals, and the P1 peptide has been tethered to other intercalators.

Apart from mutating the original P1 peptide, we have looked to naturally occurring restriction enzymes as a basis for a new design. Specifically, a short β hairpin was excerpted from the *Bam*HI restriction endonuclease and tethered to the $[Rh(phi)_2bpy']^{3+}$ intercalator (Figure 1). *Bam*HI binds to DNA as a dimer and cleaves at 5′-GGATCC-3′ palindromic sites to give four base 5′ staggered ends. Three important catalytic residues (Asp94, Glu111, and Glu113) have been identified through mutagenesis studies and analysis of the crystal structure (*29*). These residues are found clustered on the β4 and β5 strands of a β meander and are incorporated into our short synthetic peptide. Although the mechanism of the enzyme is still under investigation, evidence from recent crystallographic studies suggests that the residues coordinate and position one or two magnesium ions in the active site of the enzyme (*29*, *30*).

In addition to pursuing conjugates for hydrolysis of DNA, we have also explored the ability of P1 and a shorter histidine-containing peptide to deliver copper to DNA for oxidative cleavage. Efficient and reproducible oxidative

[1] Abbreviations: phi, 9,10-phenanthrenequinone diimine; bpy′, 4-(butyric acid)-4′-methyl-2,2′-bipyridine; bpy″, 4-(valeric acid)-4′-methyl-2,2′-bipyridine; chrysi, 5,6-chrysenequinone diimine; phen, 1,-10-phenanthroline; Rh−chrysi−P1, $[Rh(phen)(bpy''\text{-}P1)(chrysi)]^{3+}$; Pu, purine; Py, pyrimidine; DMF, *N*,*N*-dimethylformamide; PyBOP, (benzotriazol-1-yloxy)tris(pyrrolidino)phosphonium hexafluorophosphate; MPA, 3-mercaptopropionic acid; TFA, trifluoroacetic acid.

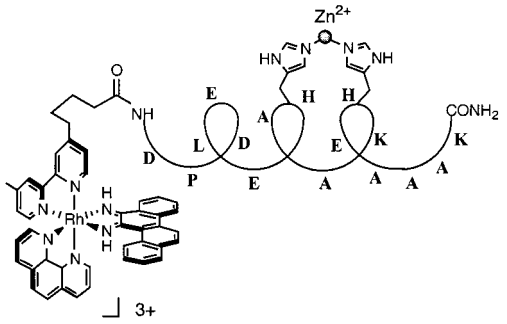

FIGURE 2: Schematic illustration of a metallointercalator−peptide conjugate, [Rh(phen)(bpy″-P1)(chrysi)]$^{3+}$, that binds preferentially at mismatch sites in DNA. The bulky chrysi ligand is better accommodated at thermodynamically destabilized sites in the helix.

cleavage of linear DNA is easier to achieve than hydrolytic cleavage, and it has been possible to perform systematic copper cleavage studies on restriction fragments from pUC19 using Rh−peptide conjugates. Not only do these Cu^{2+}-binding conjugates represent a new tool for DNA strand scission, but they also help us to characterize the interactions of our tethered peptides with DNA. By comparison of [Rh(phi)$_2$bpy′]$^{3+}$ photocleavage patterns with copper cleavage patterns, it is possible to determine the site of intercalation relative to the site of metallopeptide-promoted oxidation.

Finally, in an effort to design a sequence-selective artificial nuclease, we have attached P1 to an intercalating rhodium complex that has been demonstrated to selectively recognize mismatch sites in DNA (Figure 2). The 5,6-chrysenequinone diimine (chrysi) intercalator has an additional aromatic ring compared to the phi intercalator, and this larger intercalator binds preferentially at positions in DNA that are destabilized by mismatched base pairs (*31*−*33*).

MATERIALS AND METHODS

Synthesis of Metal Complexes. The bpy′ ligand and [Rh(phi)$_2$bpy′]Cl$_3$ complex were synthesized according to published methods (*34*−*36*). The bpy″ ligand [bpy″ = 4-(valeric acid)-4′-methyl-2,2′-bipyridine], which contains one more methylene unit than bpy′, was obtained by coupling the deprotonated 4,4′-dimethyl-2,2′-bipyridyl with an ortho ester. The ortho ester [1-(3-bromopropyl)-4-methyl-2,6,7-trioxabicyclo[2.2.2]octane] was prepared as described in the literature (*37*). The coupling product was converted to the ester by hydrolysis with $NaHSO_4$, and the desired acid was obtained by saponification with KOH. The synthesis of bpy″ gave average single-step yields of 85%. The [Rh(phen)(bpy″)(chrysi)]Cl$_3$ complex (phen = 1,10-phenanthroline) was synthesized by combining [Rh(phen)(chrysi)(NH$_3$)$_2$]$^{3+}$ (*38*) and bpy″ in a 1:1 solution of ethanol and water and refluxing overnight. The complex was purified on a Sephadex SP-C25 cation exchange column (eluted with 0.2 M $MgCl_2$), desalted with a Waters Sep-Pak C18 cartridge, and lyophilized to give a fluffy brown solid in low yield (25%). MS (electrospray): 807 (M − 3Cl − 2H$^+$), 404 (M − 3Cl − H$^+$). UV−vis (water): λ_{max} 268, 301 (shoulder), 313 (shoulder), 390, 464 nm (shoulder).

Preparation of Intercalator−Peptide Conjugates. Peptides were prepared by the Beckman Institute Biopolymer Synthesis Center at the California Institute of Technology using an ABI433 peptide synthesizer and *N*-Fmoc-L-amino acids. A 2% solution of 1,8-diazabicyclo[5.4.0]undec-7-ene in *N*,*N*-dimethylformamide (DMF) was used to deprotect the N-terminus. The resin-bound peptides were combined with racemic [Rh(phi)$_2$bpy′]Cl$_3$ or [Rh(phen)(bpy″)(chrysi)]Cl$_3$ (1−2 equiv), PyBOP (3 equiv), and diisopropylethylamine (6 equiv) in DMF and stirred at ambient temperature overnight. The conjugates were cleaved from the resin and deprotected with a cocktail of trifluoroacetic acid, water, and ethanedithiol. Peptides were prepared with a carboxamide at the C-terminus except for AHAAHA. The intercalator−peptide conjugates were HPLC purified on a semipreparative Vyadac C18 reversed phase column using a water (0.1% TFA)/acetonitrile (0.1% TFA) gradient and a flow rate of 4 mL/min. The percentage of acetonitrile was increased from 15 to 40% over the course of 20 min. Chromatograms were monitored at 220 and 360 nm. After lyophilization, the intercalator−peptide conjugates were obtained as fluffy orange solids in 2−10% yield.

Characterization of Intercalator−Peptide Conjugates. The spectral characteristics of the metal−peptide complex as determined by UV−visible spectroscopy and NMR have been found generally to be the sum of those of the intercalator and the peptide separately (*39*, *40*). The absorption of [Rh(phi)$_2$bpy′]$^{3+}$ in the UV−visible region (ϵ = 23 600 M^{-1} cm^{-1} at 349 nm) provides a convenient handle for quantification. MALDI and ESI mass spectrometry were used to verify the identity of the chimeras. Amino acid analysis confirmed both the quality of the peptide synthesis and a 1:1 ratio of peptide to metallointercalator. Potentiometric titrations were performed by adding 2 μL aliquots of 10 mM NaOH to aqueous solutions of the metallointercalator−peptide conjugate (600 μL, 100−200 μM) with constant stirring. The pH was monitored using a Beckman ϕ45 pH meter. Circular dichroism experiments were conducted using a Jasco-600 spectropolarimeter. The percent helicity was calculated according to the method of Lehrman et al. (*41*).

Plasmid Hydrolysis Experiments. Plasmid (pBR322 or pUC19) was purchased or was amplified and isolated from competent cells (DH5α or Bluescript) using a QIAGEN kit. During the plasmid isolation, the eluted DNA solution was treated with Chelex resin (Bio-Rad, 100) to remove metal ions. The plasmid cleavage properties of the intercalator−peptide conjugates were investigated by combining buffer (sodium borate or HEPES), divalent metal cation, and the intercalator−peptide conjugate with either pBR322 or pUC19 and incubating at 37 °C for 24−48 h. Typical reactions were carried out at 5 μM Rh−peptide and 40 μM bp DNA, with the pH ranging between 6 and 8, and with the divalent metal concentration varied from 1 to 50 μM. The resulting cleavage products were electrophoresed on 1% agarose gels, stained with ethidium bromide, and visualized with UV light. The kinetics of the reaction were determined by monitoring the disappearance of supercoiled plasmid with time. The amount of cleavage was quantitated using a densitometer, and pseudo-first-order rate constants (k_{obs}) were evaluated from the slope of the plot of the natural log of the ratio of supercoiled plasmid to total plasmid as a function of time. The uncertainty in rate constants was <8%.

Photocleavage, Zinc Cleavage, and Copper Cleavage Experiments with Oligonucleotides. Complementary 42-mer strands (labeled strand, 5′-CGA TGC GTA CGC GGT ATA TGC GGC ATA TGC GAA CTA TGG CAG) and 25-mer

strands with a single CC mismatch (labeled strand, 5′-GGT CAG AAT CGA CCG CAA TCA C-3′, mismatch at the underlined base) were prepared on an ABI 392 DNA synthesizer and purified by HPLC. The oligonucleotide strands were 5′ radiolabeled by reaction with T4 polynucleotide kinase and [γ-^{32}P]ATP. The labeled strand was annealed with the unlabeled complement strand by cooling from 90 °C over the course of 90 min.

To study Rh−P1 photocleavage, the 42-mer duplex (40 μM bp) was combined with either $[Rh(phi)_2bpy']^{3+}$ or the Rh−P1 conjugate (0.5−2.0 μM) in sodium cacodylate (20 mM, pH 6.8). After incubation for 15 min at 37 °C, the samples were irradiated at 313 nm for 8 min with a 1000 W Hg/Xe lamp equipped with a monochromator. For Rh−P1-mediated Zn^{2+} cleavage, reactions were carried out with 42-mer duplex (40 μM bp), the Rh−P1 conjugate (5 μM), and $ZnCl_2$ (5 μM) in sodium borate buffer (20 mM, pH 7). The samples were incubated for 24 h at 37 °C.

For Rh−chrysi−P1 photocleavage experiments, the 25-mer duplex with a CC mismatch (100 μM bp) was combined with $[Rh(phen)(bpy'')(chrysi)]^{3+}$ or the Rh−chrysi−P1 conjugate (5 μM) in Tris-HCl buffer (25 mM, pH 7.5). After incubation for 15 min at ambient temperature, the samples were irradiated at 365 nm for 15 min. To study Rh−chrysi−P1-mediated Zn^{2+} cleavage, the 25-mer duplex (100 μM bp) was reacted with $ZnCl_2$ (5 μM) and either $[Rh(phen)(bpy'')(chrysi)]^{3+}$ or the Rh−chrysi−P1 conjugate (5 μM) in sodium borate buffer (25 mM, pH 6). The samples were incubated for 40 h at 37 °C. To study Rh−chrysi−P1-mediated Cu^{2+} cleavage, the labeled 25-mer duplex (100 μM bp) was combined with $CuCl_2$ (50 μM), 3-mercaptopropionic acid (MPA, 500 μM), and $[Rh(phen)(bpy'')(chrysi)]^{3+}$ or the Rh−chrysi−P1 conjugate (5 μM) in Tris-HCl buffer (25 mM, pH 7.5). The samples were incubated at 37 °C for 24 h.

The samples from photocleavage, Zn^{2+}, and Cu^{2+} cleavage experiments were dried, resuspended in formamide loading dye, and analyzed by 20% PAGE. Gels were visualized by phosphorimagery.

Photocleavage and Copper Cleavage Experiments with Restriction Fragments. A restriction fragment with radiolabel incorporated at the 3′-termini of one strand was prepared by digesting pUC19 with *Bam*HI, labeling with the Klenow fragment of *Escherichia coli* Pol I and [α-^{32}P]dGTP, and then digesting with *Bgl*I. The labeled fragment was isolated from a 6% nondenaturing PAGE gel and was desalted on a C18 cartridge.

For Rh−peptide-mediated photocleavage experiments, the labeled fragment was combined with carrier DNA (calf thymus, 100 μM bp), the Rh−peptide conjugate, and Cu^{2+} (1:1 with the metal−peptide conjugate) in Tris-HCl buffer (25 mM, pH 7.85). The samples were irradiated for 5 min at 313 nm. To study intercalator−peptide copper cleavage, the labeled fragment was combined with carrier DNA (calf thymus, 100 μM bp), the Rh−peptide conjugate, Cu^{2+} (20 μM), and MPA (200 μM) in Tris-HCl buffer (25 mM, pH 7.85). Reaction mixtures were incubated at ambient temperature for 4 h. Photocleavage and copper cleavage reaction samples were dried under vacuum, suspended in formamide loading dye, and analyzed by 8% PAGE. Gels were visualized by phosphorimagery and quantitated using ImageQuant software.

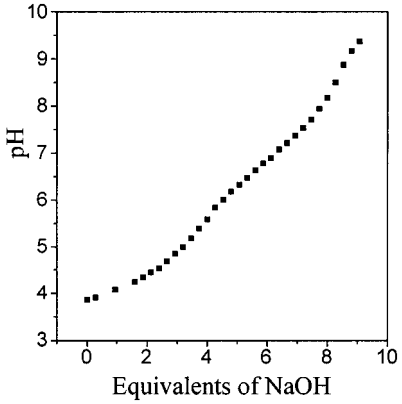

FIGURE 3: Potentiometric titration of the Rh−P1 conjugate. The pH of a 165 μM solution of the Rh−P1 conjugate was monitored as the solution was titrated with 10 mM NaOH. The broad inflection centered around pH 6.8 corresponds to the deprotonation of the two histidine residues and the phi ligands.

RESULTS

Characterization of Metal−Peptide Conjugates by pH Titration and Circular Dichroism. Potentiometric titration of the Rh−P1 conjugate (165 μM) gave a titration curve with three broad inflections corresponding to deprotonation of acidic residues, histidine residues and immine protons of the phi ligand, and lysine residues. Because of the overlapping titration regimes, a rigorous fit of the titration curve was not possible. Instead, the pK_a of histidine was estimated by analyzing the slope of the curve. The curve showed an inflection centered around pH 6.8 (Figure 3). This corresponds to the deprotonation of the histidine residues and the deprotonation of the phi ligand. The pK_a of the phi imine proton in $[Rh(phi)_2bpy]^{3+}$ is ∼6.8−6.9, and this shifts the inflection to pH values that are higher than would be expected for histidine alone and broadens the inflection (*42*). There was no evidence of precipitation when the Rh−P1 conjugate was titrated in the absence of Zn^{2+}. However, during the titration with dilute sodium hydroxide in the presence of zinc ion, a black precipitate began to form as the pH was increased above 7.5. Potentiometric titration of the Rh−Bam conjugate (100 μM) in the presence of Zn^{2+} (100 μM) resulted in significant precipitation of the orange complex between pH 3.5 and 4.5. As the pH was increased to 8, the orange precipitate dissolved and a black precipitate began to form. Because of the complications of precipitation, Zn^{2+} affinities could not be determined by this method.

The helical content of the Rh−P1 variants was explored by circular dichroism (Figure 4). The rhodium−peptide derivatives of the Rh−P1 conjugate (Table 1) that contain two histidines in the *i* and *i* + 4 positions (Rh−P2, Rh−P3, and Rh−P5) behaved much like the Rh−P1 conjugate. The calculated helicity was modest for all of these conjugates, ranging from 12 to 22%, and increased slightly with the addition of Zn^{2+}. The extent of helical induction is comparable to the low level of induction previously reported for designed Zn^{2+}-coordinating peptides (*43*). With the Rh−P1, Rh−P3, and Rh−P5 conjugates, the helical content reached a maximum at stoichiometric zinc. This was a very small effect, but was consistently observed. In contrast, the conjugate without histidine residues (Rh−P4) demonstrated the highest helical content in the absence of Zn^{2+}; the addition of Zn^{2+} to the Rh−P4 conjugate actually caused a

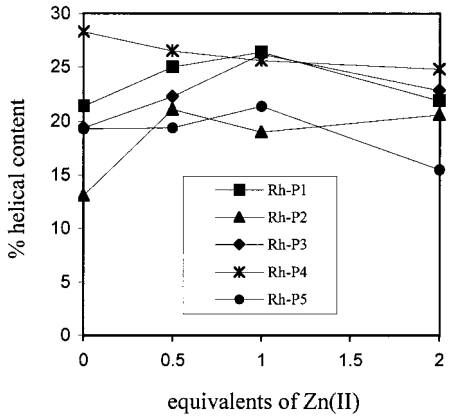

FIGURE 4: Plot of the α helical content as a function of Zn^{2+} concentration for five Rh−P1 variants. CD spectra were obtained for Rh−peptide complexes (2−4 μM) in sodium borate buffer (20 mM, pH 7).

Table 1: Variations on the Rh−P1 Conjugate[a]

Rh−P1	Rh−DPDELE**H**AAK**H**EAAAK-$CONH_2$
Rh−P2	Rh−DPDALE**H**AAK**H**EAEAK-$CONH_2$
Rh−P3	Rh−DPDELE**H**AAK**H**EAEAK-$CONH_2$
Rh−P4	Rh−DPDELEEAAKEEAEAK-$CONH_2$
Rh−P5	Rh−DPDALE**H**AAK**H**EAAAK-$CONH_2$
Rh−P6	Rh−DPDE*LE**H**AAK**H**EAAAK-$CONH_2$
Rh−P7	Rh−DPDE**LE**H**AAK**H**EAAAK-$CONH_2$

[a] E* is α-aminoadipic acid and E** α-aminosuberic acid.

slight decrease in helicity. The Rh−P1 conjugate exhibited different behavior when titrated with Cu^{2+} instead of Zn^{2+}. Helicity increased with the addition of copper, but in contrast to results obtained with Zn^{2+}, it did not decrease as the amount of Cu^{2+} was increased from 1 to 5 equiv (data not shown). The circular dichroism studies of the Rh−Bam conjugate did not provide any information about the conformation of the tethered peptide. No features characteristic of helices or β hairpins were observed in the CD spectrum of the Rh−Bam conjugate, and no significant changes occurred in the spectrum on titration with Zn^{2+} (data not shown). It is possible that association with DNA may help to organize these small rhodium-tethered peptides; the strong absorptivity of DNA in the ultraviolet region, however, interferes with the characterization of any DNA-promoted stabilization by CD (*44*).

DNA Plasmid Cleavage with the Rh−P1 Conjugate and Zinc. The Rh−P1 conjugate converts supercoiled plasmid (I) to nicked (II) and linear forms (III) in the presence of Zn^{2+} (*25*). The results of plasmid cleavage experiments with the Rh−P1 conjugate are summarized in Table 2. The metallointercalator, the tethered peptide, and the divalent cation were all essential for efficient cleavage of pBR322. If one of these components was absent, only a modest increase in the percentage of nicked plasmid (form II_M) relative to that in a control reaction was observed. The metallointercalator alone, $[Rh(phi)_2bpy']^{3+}$, provided a slight increase in the amount of nicked plasmid in the absence or presence of Zn^{2+}, but it was certainly much less effective than the Rh−P1 conjugate and Zn^{2+} in the cleavage of supercoiled plasmid (note the percentage of form I remaining). The Rh−P1 conjugate was relatively ineffective without added metal or in the presence of a metal scavenger such as EDTA. The data also emphasize the importance of a 1:1 conjugate:Zn^{2+} stoichiometry. The percentage of linear plasmid (form III) was highest at 1.0 equiv of Zn^{2+}.

Table 2: Cleavage of Supercoiled Plasmid pBR322 DNA by the Rh−P1 Conjugate

conditions[a]	% I_M	% II_M	% III_M
control	82	18	
$[Rh(phi)_2bpy']^{3+}$	65	35	
P1 with Zn^{2+}	72	28	
Rh−P1 with EDTA	69	31	
Rh−P1	56	40	4
Rh−P1 with 0.5 equiv of Zn^{2+}	17	53	30
Rh−P1 with 1.0 equiv of Zn^{2+}	18	44	38
Rh−P1 with 2.0 equiv of Zn^{2+}	44	39	17
Rh−P1 with 4.0 equiv of Zn^{2+}	45	41	14
Zn^{2+}	65	31	4
Rh−P1 with 1.0 equiv of Cd^{2+}	50	50	
Cd^{2+}	81	19	
Rh−P1 with 1.0 equiv of Cu^{2+}	55	45	
Cu^{2+}	50	50	
Rh−P1 with 1.0 equiv of Fe^{2+}	20	80	
Fe^{2+}	70	30	

[a] All experiments were conducted using pBR322 DNA (32 or 40 μM bp) in sodium borate buffer (20 mM, pH 7). Tabulated are the additional reagents that were used at 5 μM unless otherwise noted. The samples were incubated for 24 h at 37 °C. The amounts of supercoiled (I_M), nicked (II_M), and linear (III_M) monomer were quantitated, and the results of several trials were averaged. Variations of 5−10% were evident between experiments.

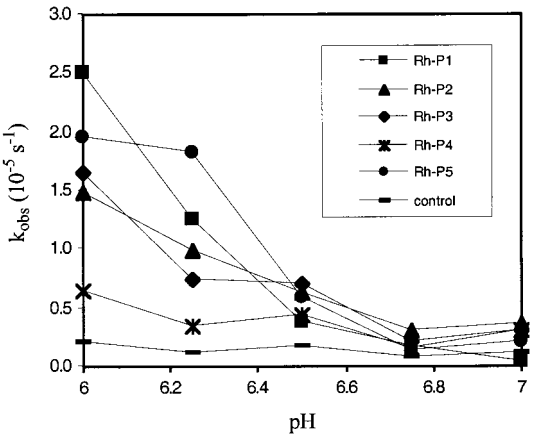

FIGURE 5: Pseudo-first-order rate constant plotted vs pH for five Rh−P1 variants. The reactions were carried out with pBR322 DNA (40 μM bp), the rhodium−peptide conjugate (5 μM), and $ZnCl_2$ (5 μM) in sodium borate (20 mM) at 37 °C.

Although the results presented in Table 2 are typical, the Rh−P1 conjugate did not promote plasmid cleavage in every experiment. When plasmid cleavage was observed, the level of cleavage was quite consistent (hence, the reasonable errors for the data in Table 2). Yet even under the conditions best suited for Rh−P1 hydrolysis (pH 6 and stoichiometric Zn^{2+}), cleavage of the plasmid was not always achieved. This irreproducibility seems to be largely due to the solubility of Zn^{2+} and to the sensitivity of the Rh−P1 conjugate to Zn^{2+} concentration. Careful attention to buffer, metal ion, and plasmid preparation did not completely resolve this problem.

DNA Plasmid Cleavage with Rh−P1 Variants and Zinc. The Rh−P1 mutants were tested against the original Rh−P1 conjugate in plasmid cleavage experiments. Pseudo-first-order rate constants were determined for five conjugates between pH 6 and 7 (Figure 5). For all conjugates, the rate constant was highest at pH 6. At pH 6, the values for the

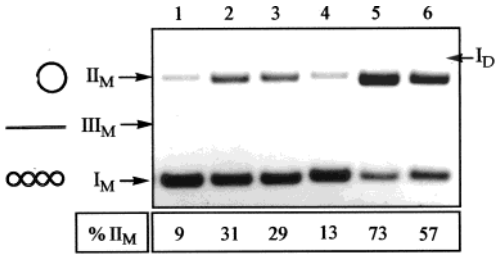

FIGURE 6: Rh−Bam-promoted cleavage of supercoiled pUC19. The reactions were carried out with pUC19 (40 μM), the Rh−Bam conjugate (5 μM), and $ZnCl_2$ in HEPES (20 mM, pH 6) for 24 h at 37 °C. The reactions were analyzed by agarose gel electrophoresis: lane 1, DNA alone; lane 2, DNA with 5 μM $ZnCl_2$; lane 3, DNA with 500 μM $ZnCl_2$; lane 4, DNA with the Rh−Bam conjugate; lane 5, DNA with the Rh−Bam conjugate and 5 μM $ZnCl_2$; and lane 6, DNA with the Rh−Bam conjugate and 500 μM $ZnCl_2$. The supercoiled monomer (I_M), nicked monomer (II_M), and linear monomer (III_M) are labeled. A very small amount of supercoiled dimer (I_D) is also labeled. The percentage of nicked plasmid is presented below each lane.

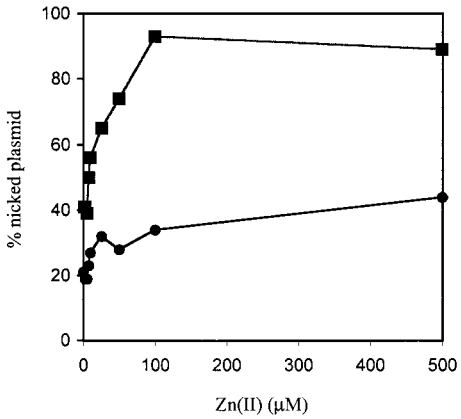

FIGURE 7: Changes in Rh−Bam cleavage with increasing $ZnCl_2$ concentrations. The percentage of nicked plasmid is plotted vs $ZnCl_2$ concentration for reactions with 5 μM Rh−Bam conjugate (■) and control reactions without the Rh−Bam conjugate (●). The reactions were carried out with 40 μM pBR322 in sodium borate buffer (25 mM, pH 6) at 37 °C for 24 h.

Rh−P2, Rh−P3, and Rh−P5 conjugates were very close to that observed for the Rh−P1 conjugate. Only the conjugate without histidine (Rh−P4) exhibited a significantly lower rate of plasmid cleavage. Although rate constants were not determined for the Rh−P6 and Rh−P7 conjugates, they were found to give lower cleavage levels than the Rh−P1 conjugate in plasmid assays.

DNA Plasmid Cleavage with the Rh−Bam Conjugate and Zinc. The Rh−Bam conjugate was tested in plasmid cleavage assays to determine if the short Bam peptide could still promote DNA hydrolysis outside of its protein architecture. As can be seen in Figure 6, like the Rh−P1 conjugate and its derivatives, the Rh−Bam conjugate converted supercoiled plasmid to a nicked form in the presence of Zn^{2+}. Tethering the Bam peptide to a metallointercalator and including divalent cation in the reaction mixture were both essential for effective cleavage. As was observed for the entire family of Rh−P1 conjugates, the Rh−Bam conjugate cleaved plasmid most effectively at pH 6. Like the Rh−P1 conjugate, the Rh−Bam conjugate sometimes failed to cleave plasmid substrates even under optimized conditions; indeed, with the Rh−Bam conjugate, the problem seems to be aggravated by reduced conjugate solubility relative to that of the Rh−P1 conjugate.

There were also some notable differences in the cleavage properties of the Rh−P1 and Rh−Bam conjugates. The Rh−Bam conjugate continued to promote effectively DNA cleavage as the zinc ion concentration increased beyond stoichiometric levels, whereas the Rh−P1 cleavage levels dropped significantly above 1 equiv of Zn^{2+}. In one set of reactions with the Rh−Bam conjugate, the Zn^{2+} concentration was varied between 2.5 (0.5 equiv) and 500 μM (100 equiv) (Figure 7). The percentage of nicked plasmid steadily increased with zinc ion concentration to 100 μM and then decreased slightly at higher concentrations. Notably, at millimolar Zn^{2+} concentrations, the Rh−Bam conjugate was no longer essential for delivery of the cation to DNA, and Zn^{2+} alone produced a significant population of nicked plasmid (data not shown).

Importantly, and in contrast to the Rh−P1 conjugate, the Rh−Bam conjugate has not been demonstrated to cleave linear oligonucleotide DNA. The Rh−Bam conjugate has been tested with a variety of oligonucleotide substrates, but despite parallel experiments that gave as much as 90% conversion of plasmid to a nicked form, no damage to an oligonucleotide substrate was observed. It is also noteworthy that very little linear plasmid was produced in the Rh−Bam reaction with supercoiled plasmid DNA; in fact, in reactions that produced 60−70% nicked plasmid (Figure 6), no linear plasmid was observed.

Plasmid Cleavage Experiments with a Variety of Redox and Non-Redox-Active Metals. The Rh−P1 conjugate was tested with a variety of divalent cations in plasmid cleavage experiments (Table 2). We observed an increase in the percentage of nicked plasmid relative to that in control reactions when Cd^{2+} and the Rh−P1 conjugate were incubated with pBR322; however, the cleavage levels were considerably lower than those achieved with Zn^{2+}, and there was no significant formation of linear plasmid. Interestingly, the Rh−P1 conjugate actually moderated the percentage of nicked plasmid produced by incubation with Cu^{2+}. Micromolar concentrations of copper ion alone gave 50% nicked plasmid, presumably by an oxidative reaction, but in the presence of the Rh−P1 conjugate, the percentage of nicked plasmid decreased. In contrast, with Fe^{2+}, the addition of the Rh−P1 conjugate significantly increased the percentage of nicked plasmid compared to reactions with Fe^{2+} alone; 80% nicked plasmid, but no linear plasmid, was observed. Again, the efficient Fenton chemistry associated with Fe^{2+} makes a hydrolytic mechanism unlikely.

Similar cleavage results were observed for the Rh−Bam conjugate when it was tested with a variety of metal ions (Table 3). Cadmium ion gave cleavage results that were comparable to those achieved with Zn^{2+}, and Mg^{2+}, the cation used in the active site of the *Bam*HI restriction enzyme, exhibited lower cleavage activity than Zn^{2+}. As was observed for the Rh−P1 conjugate, copper cleavage was curbed by the addition of the Rh−Bam conjugate. At 1 equiv of Fe^{2+}, there appeared to be a slight gain in the level of cleavage in the presence of the Rh−Bam conjugate, but at higher concentrations of Fe^{2+}, the plasmid was effectively fragmented even without the addition of the Rh−Bam conjugate.

Oligonucleotide DNA Cleavage with the Rh−P1 Conjugate and Zn^{2+}. Importantly, the Rh−P1 conjugate cleaves

Table 3: Cleavage of Supercoiled Plasmid pBR322 DNA by the Rh−Bam Conjugate

conditions[a]	% I_M	% II_M	% III_M
control	74	26	
Rh−Bam	62	38	
Rh−Bam with 100 equiv of Zn^{2+}	44	54	2
Zn^{2+}	78	22	
Rh−Bam with 100 equiv of Cd^{2+}	39	57	4
Cd^{2+}	76	24	
Rh−Bam with 100 equiv of Mg^{2+}	59	41	
Mg^{2+}	84	16	
Rh−Bam with 1 equiv of Cu^{2+}	40	54	6
Rh−Bam with 100 equiv of Cu^{2+}	35	62	3
Cu^{2+} (5 μM)	0	90	10
Cu^{2+} (500 μM)	0	52	48
Rh−Bam with 1 equiv of Fe^{2+}	63	35	2
Rh−Bam with 100 equiv of Fe^{2+}			fragments
Fe^{2+} (5 μM)	77	21	2
Fe^{2+} (500 μM)			fragments

[a] All experiments were conducted using pBR322 DNA (40 μM bp) in sodium borate buffer (25 mM, pH 6). Tabulated are the additional reagents that were used. The concentration of the Rh−Bam conjugate was 5 μM, and the concentration of the divalent cation was 500 μM unless otherwise noted. The samples were incubated for 24 h at 37 °C. The amounts of supercoiled (I_M), nicked (II_M), and linear (III_M) monomer were quantitated, and the data are reported from a single set of experiments.

not only supercoiled substrates but also linear oligonucleotides. With these DNA substrates, it is possible to characterize the products and the specificity of hydrolysis activity through high-resolution gel electrophoresis. Moreover, the photocleavage reaction mediated by $[Rh(phi)_2bpy']^{3+}$ provides a convenient method for determining the intercalation sites of the Rh−P1 conjugate. By comparing photocleavage patterns and hydrolysis patterns, we gain structural insight into the interactions of the intercalator−metallopeptide conjugate with DNA.

The radiolabeled 42-mer duplex was irradiated in the presence of $[Rh(phi)_2bpy']^{3+}$ or the Rh−P1 conjugate, and the sites of DNA damage were revealed by dark bands in the imaged gel. The pattern of damage suggested essentially sequence-neutral binding of both the rhodium complex and the Rh−P1 conjugate. Photocleavage occurred over the entire sequence with only a modest selectivity for 5′-Pu-*Py*-Pu-Py-3′ sites (cleavage at *Py*, Figure 8A). Tethering the peptide to $[Rh(phi)_2bpy']^{3+}$ did not dramatically change the photocleavage properties of the rhodium complex (in Figure 8A, compare lanes 3 and 4). The peptide appears to reduce the damage intensity slightly, but does not change its distribution. The appearance of double bands for the highly resolved products at the bottom of the gel is consistent with the formation of both 3′-phosphate termini and slower moving 3′-phosphoglycaldehyde termini (Figure 8A); these have been previously observed and characterized in photocleavage experiments with phi complexes of rhodium (*27*).

To achieve hydrolysis, the 42-mer duplex was incubated with the Rh−P1 conjugate and Zn^{2+}. Gel electrophoresis and imaging revealed damage of varying intensity at several sites in the duplex (Figure 8B). This damage was observed only in the presence of the Rh−P1 conjugate and not in a reaction with Zn^{2+} alone. The termini produced during the Rh−P1 reaction can be determined by comparing the migration of product bands with the migration of Maxam−Gilbert bands and dephosphorylated Maxam−Gilbert bands. Several of the product bands did most closely comigrate with the dephosphorylated Maxam−Gilbert bands (Figure 8B, indicated with arrows). This suggested the formation of 3′-hydroxyls and was consistent with previous Rh−P1 hydrolysis results with a 17-mer duplex (*25*). Again, as with plasmid cleavage studies, the Rh−P1 conjugate does not always cleave when it is incubated with oligonucleotides under the ideal conditions; in fact, achieving cleavage of short duplexes is more difficult than achieving cleavage of plasmid substrates.

Qualitative comparisons of the sites of most intense photocleavage and most intense hydrolysis damage reveal a consistent pattern of photoactivated oxidative damage at a given base and hydrolysis of the phosphodiester linkage of the adjacent 3′ base (Figure 8C). In Figure 8C, the solid arrows indicate positions of photocleaved bases and dotted arrows indicate hydrolyzed phosphodiester linkages. From previous studies, we know that $[Rh(phi)_2bpy]^{3+}$ cleaves with 5′ asymmetry (*27*), so we can assign the intercalation site on the basis of our photocleavage pattern (Figure 8C, indicated by black bars).

Linear DNA Cleavage with the Rh−P1 Conjugate and Copper. Because efficient and reproducible oxidative cleavage of linear DNA is easier to achieve than hydrolytic cleavage, we have also used our Rh−peptide conjugates to deliver redox-active metals such as Cu^{2+} to a restriction fragment of DNA. Again in these experiments, the pattern of $[Rh(phi)bpy']^{3+}$ photocleavage reveals the intercalation sites of the conjugate and the pattern of copper-mediated damage reveals the interactions of the peptide and the DNA. In the presence of Cu^{2+} and MPA, the Rh−P1 conjugate promoted oxidative strand breaks at specific locations in a plasmid restriction fragment (Figure 9, lanes 11−13). There was no damage to the DNA after incubation for 24 h with Cu^{2+} if MPA was not added to the reaction mixture (Figure 9, lane 9). Although the photocleavage pattern produced by the Rh−P1 conjugate on irradiation at 313 nm (Figure 9, lanes 3−5) suggested fairly sequence-neutral binding with some preference for 5′-Pu-*Py*-Pu-3′ sites, the copper cleavage was highly localized. There appeared to be some correlation between photocleavage and copper cleavage, but not all sites with equally intense photocleavage had corresponding sites of equally intense copper damage. The two sites that were most intensely damaged by copper were 5′-Py-Py-*Pu*-Pu-Pu-3′ sites (cleavage at *Pu*), but not all such sites were damaged.

The Rh−P1 conjugate plays a critical role in delivering the copper to the DNA, and only very low levels of damage were observed when DNA was incubated with copper and MPA alone (Figure 9, lane 7). The presence of histidine in the peptide was also essential for the copper-mediated reaction; neither $[Rh(phi)_2bpy']^{3+}$, the Rh−Bam conjugate, nor the Rh−P4 conjugate promoted damage to the restriction fragment under identical conditions (data not shown).

The pattern of copper damage changed when P1 was replaced with a much shorter histidine-containing peptide. A hexamer peptide (AHAAHA) was tethered to $[Rh(phi)_2bpy']^{3+}$ and was incubated with the restriction fragment, Cu^{2+}, and MPA (Figure 10). The photocleavage pattern observed for this conjugate was very similar to the pattern observed for the Rh−P1 conjugate (Figure 10, lanes 3−5), and again the pattern suggested sequence-neutral binding to the DNA. The copper damage with the Rh−AHAAHA

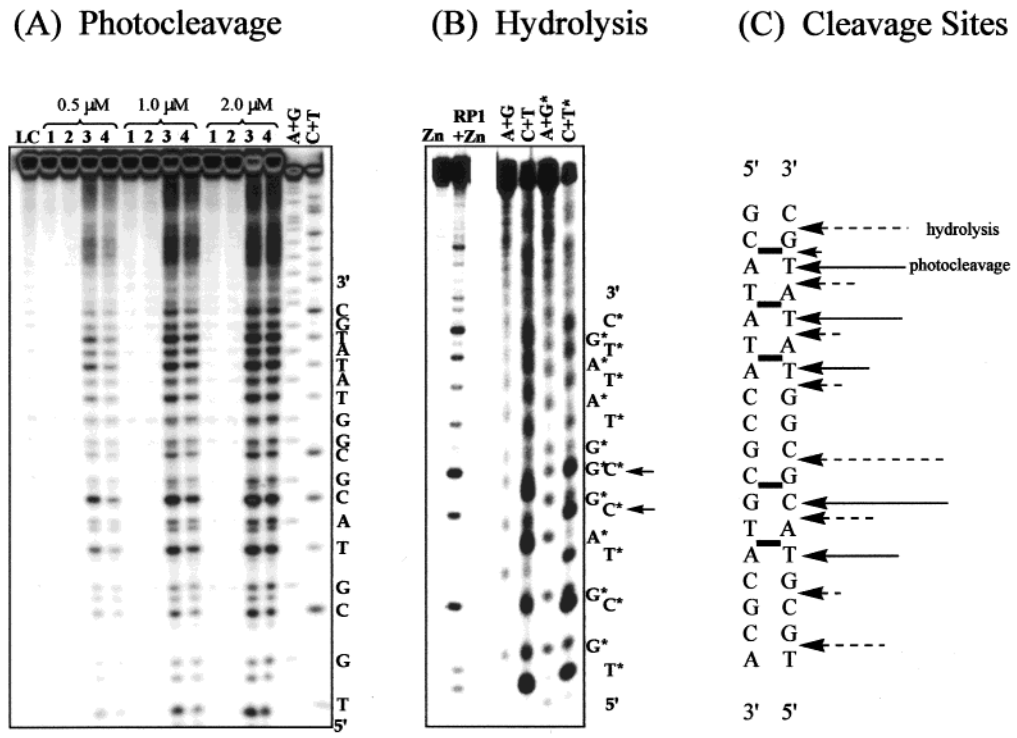

FIGURE 8: Rh−P1 photocleavage and Zn^{2+}-promoted hydrolysis of a 42 bp oligonucleotide DNA. (A) Photocleavage of a 42 bp duplex by $[Rh(phi)_2bpy']^{3+}$ and the Rh−P1 conjugate. The concentrations of $[Rh(phi)_2bpy']^{3+}$ and the Rh−P1 conjugate are indicated: A+G and C+T, Maxam−Gilbert sequencing lanes; LC, light control, irradiation without the Rh complex; lane 1, $[Rh(phi)_2bpy']^{3+}$, no irradiation; lane 2, the Rh−P1 conjugate, no irradiation; lane 3, irradiation with $[Rh(phi)_2bpy']^{3+}$; and lane 4, irradiation with the Rh−P1 conjugate. (B) Hydrolysis of a 42 bp duplex by the Rh−P1 conjugate and Zn^{2+}. Dephosphorylated Maxam−Gilbert products are indicated with an asterisk. Damage to the DNA is observed only in a reaction with the Rh−P1 conjugate and Zn^{2+}, and not in a reaction with Zn^{2+} alone. (C) Qualitative comparison of sites of photocleavage and sites of hydrolysis on a 42-mer duplex. The solid arrows denote the five bases that showed the most photocleavage damage. The dashed arrows denote the phosphodiester linkages that were cleaved hydrolytically. The lengths of the arrows are rough estimates of the relative amounts of a single type of cleavage, but no relationship between the efficiency of photocleavage and hydrolytic cleavage is implied. The black bars show the sites of intercalation of the rhodium complex derived from the photocleavage pattern.

conjugate was not as dramatically localized to specific sites as with the Rh−P1 conjugate, and the peaks in damage produced by the Rh−AHAAHA conjugate were not observed at precisely the same positions as the peaks in damage produced by the Rh−P1 conjugate (Figure 10, lanes 11−13). With both the Rh−P1 and Rh−AHAAHA conjugates, there seemed to be a slight preference for copper damage at flexible AT-rich sequences.

Selectively Targeting Mismatches: Photocleavage, Cu^{2+} Cleavage, and Zn^{2+} Cleavage Experiments with [Rh(phen)(bpy″-P1)(chrysi)]$^{3+}$. To mimic a site-selective nuclease, we attached P1 to an intercalating rhodium complex that specifically recognizes mismatches (Figure 2). The [Rh(phen)(bpy″)(chrysi)]$^{3+}$ complex contains a large 5,6-chrysenequinone diimine intercalator and is not well accommodated at standard Watson−Crick base pairs. This rhodium complex binds preferentially at base−base mismatches which destabilize the DNA helix, and like $[Rh(phi)_2bpy]^{3+}$, the complex can be photoactivated to cleave at the DNA binding site (*31*−*33*).

To test the binding and selectivity of the Rh−chrysi−P1 conjugate, the complex was irradiated with a 25-mer duplex containing a CC mismatch (Figure 11). Attachment of P1 did not change the selectivity of the chrysi complex for mismatch sites. As with unfunctionalized [Rh(phen)(bpy″)(chrysi)]$^{3+}$ and $[Rh(bpy)_2(chrysi)]^{3+}$, the conjugate gave pronounced photocleavage only at the bases to the 3′ side of the mismatch (Figure 11, lane 5). As was observed with the Rh−P1 conjugate, the peptide slightly reduced the photocleavage intensity but did not change the pattern of damage.

The Rh−chrysi−P1 complex was incubated with Zn^{2+} and the 25-mer substrate, but even after incubation for 40 h, there was no damage observed near the mismatch site or at any other site in the duplex (Figure 11, lanes 19 and 20). Incubation of the 25-mer duplex with the Rh−chrysi−P1 conjugate in the presence of Cu^{2+} and MPA also produced very little damage near the CC mismatch site. There was a very slight increase in the amount of copper-mediated damage at the CC base pair, but this increase depended only on the presence of the rhodium intercalator and not on the appended peptide (in Figure 11, compare lanes 9 and 11). In these experiments, the intercalator alone recruits a very small amount of Cu^{2+} damage near the CC mismatch.

DISCUSSION

The delivery of metal ions to DNA is a common strategy for the hydrolysis of the phosphodiester bond. Indeed, this strategy is observed in both natural nucleases and essentially all of the reported artificial nucleases. Metal ions accelerate hydrolysis by Lewis acid activation, nucleophilic activation, and/or leaving group stabilization (*1*). Our approach to targeting the DNA backbone also takes advantage of metal

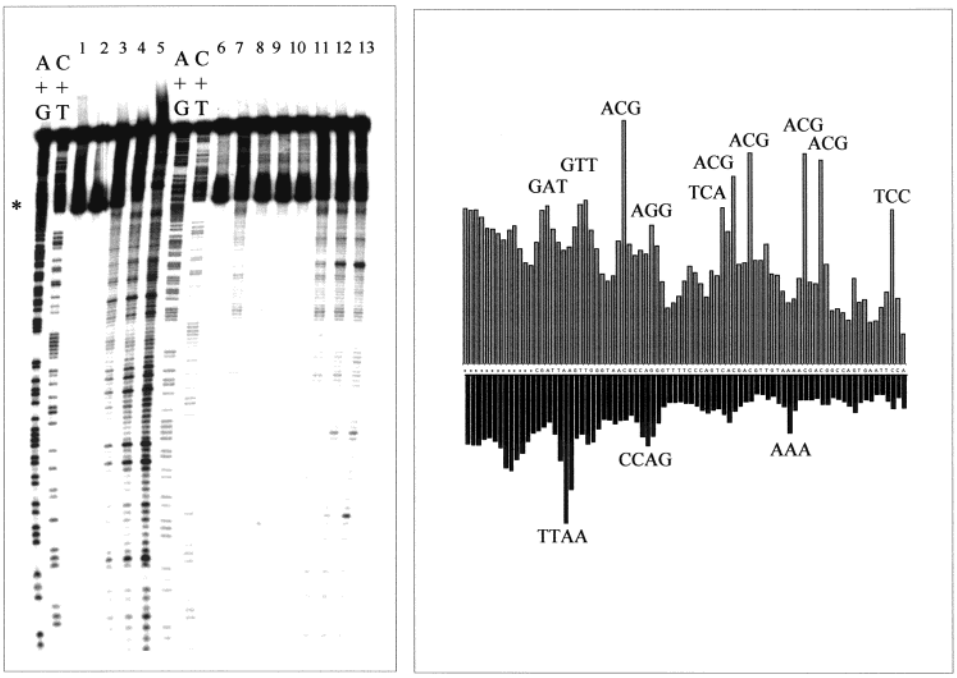

FIGURE 9: Rh−P1 photocleavage and copper cleavage of a restriction fragment. Left panel: lane 1, irradiation of DNA without the Rh−peptide conjugate; lane 2, 10 μM Rh−peptide conjugate, no irradiation; lanes 3−5, increasing Rh−peptide conjugate concentrations (2, 5, and 10 μM, respectively), irradiation for 5 min; lane 6, DNA alone, 4 h at room temperature (RT); lane 7, Cu^{2+} with MPA, 4 h at RT; lane 8, 10 μM Rh−peptide conjugate with Cu^{2+} (no MPA), 4 h at RT; lane 9, 10 μM Rh−peptide conjugate Cu^{2+} (no MPA), 24 h at 37 °C; lane 10, 10 μM Rh−peptide conjugate, 4 h at RT; and lanes 11−13, increasing concentrations of the Rh−peptide conjugate (2, 5, and 10 μM, respectively) with Cu^{2+} and MPA, 4 h at RT. The asterisk denotes a band that arises from renaturation of the fragment. Right panel: bar plot comparing photocleavage (top) and copper cleavage (bottom) across a segment of the restriction fragment.

ions, and in a chemically well-defined manner. Rather than employing ligands that only weakly associate with DNA, perhaps through electrostatic interactions, we have linked a peptide to a DNA-intercalating metal complex. The peptide coordinates the divalent cation, and the metallointercalator efficiently delivers both the peptide and metal ion to the DNA backbone. Our conjugate contains three essential components: (i) a peptide with residues for coordination of a divalent metal ion, (ii) the coordinated metal cation, and (iii) a DNA-binding metallointercalator. In developing different artificial nucleases, we have investigated each of these three components. Here we consider the benefits and challenges of this strategy.

The Peptide. There are both advantages and disadvantages to employing peptides to create the coordination environment for divalent cations. Through solid phase synthesis, peptides are readily prepared and purified. Since they are composed of readily available building blocks, it is facile to tune the peptide composition to achieve the desired properties and variations. A great deal of effort has been invested in the creation of short peptide systems with defined secondary structure (*45*), and the elucidated principles can be incorporated into the design of tethered peptides. Also, because we are using the ligands that enzymes use for orienting and presenting metal ions in an active site, our conjugates likely have biological relevance.

On the other hand, short peptides do not provide a rigid or well-defined coordination environment. In contrast to many of the small synthetic ligands employed in other laboratories for metal-promoted DNA hydrolysis (*11*−*14*, *23*), our peptides are very flexible. Indeed, our designed α helix is only modestly helical, and the peptide derived from the *Bam*HI enzyme shows no evidence of a β hairpin conformation by CD.

Additionally, these short peptides offer little control over the stoichiometry of metal binding, the intramolecularity of metal coordination, and the associated solubility properties. Zn^{2+} precipitates as reaction solutions approach pH 7, and our flexible peptides, with only naturally occurring amino acids, are not effective at solubilizing the Zn^{2+} ion. Additionally, depending on the composition of the peptide, solubility of the conjugate becomes an important issue. The Bam peptide is only modestly soluble, and potentiometric titrations showed precipitation of the Rh−Bam conjugate around pH 4 as the acidic groups were deprotonated. The Rh−Bam conjugate redissolved as the pH increased to 7, but at this pH, free Zn^{2+} began to precipitate. In reactions with the Rh−Bam conjugate, therefore, the pH must be carefully balanced to prevent precipitation of the conjugate or zinc ion. Despite these difficulties, DNA cleavage chemistry has been achieved with conjugates containing both the de novo-designed P1 peptide and the Bam peptide.

The Rh−P1 Conjugate and Derivatives. With the Rh−P1 conjugate, we have demonstrated hydrolysis of both plasmid and oligonucleotide DNA using micromolar concentrations of the conjugate (*25*). The pseudo-first-order rate constant for plasmid cleavage is comparable to the rate constants reported for other artificial nucleases (*23*, *24*), and is on the same order of magnitude as the acceleration predicted by Chin et al. for catalysis by leaving group activation (*1*).

A strength of the peptide strategy is the ability to vary residues systematically to assess the features of the Rh−P1 conjugate that contribute to DNA hydrolysis activity. Several

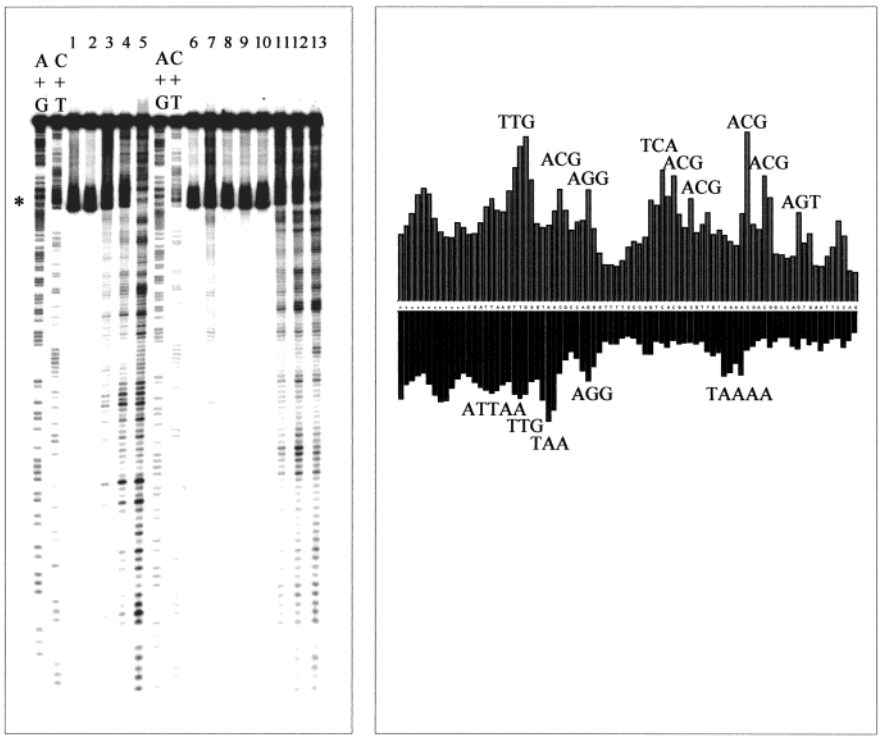

FIGURE 10: Rh−AHAAHA-COOH photocleavage and copper cleavage of a restriction fragment. Left panel: lane 1, irradiation of DNA without the Rh−peptide conjugate; lane 2, 10 μM Rh−peptide conjugate, no irradiation; lanes 3−5, increasing Rh−peptide conjugate concentrations (2, 5, and 10 μM, respectively), irradiation for 5 min; lane 6, DNA alone, 4 h at room temperature (RT); lane 7, Cu^{2+} with MPA, 4 h at RT; lane 8, 10 μM Rh−peptide conjugate with Cu^{2+} (no MPA), 4 h at RT; lane 9, 10 μM Rh−peptide conjugate with Cu^{2+} (no MPA), 24 h at 37 °C; lane 10, 10 μM Rh−peptide conjugate, 4 h at RT; and lanes 11−13, increasing concentrations of the Rh−peptide conjugate (2, 5, and 10 μM, respectively) with Cu^{2+} and MPA, 4 h at RT. The asterisk denotes a band that arises from renaturation of the fragment. Right panel: bar plot comparing photocleavage (top) and copper cleavage (bottom) across a segment of the restriction fragment.

key residues in the peptide were individually mutated, and the effects of these mutations were determined in plasmid cleavage assays. Not surprisingly, these mutations suggest that the essential feature of the Rh−P1 conjugate is the two-histidine coordination site formed by His7 and His11. From comparisons of the activities of the Rh−P1 and Rh−P4 conjugates, in which His7 and His11 were mutated to glutamates, it is clear that the histidine pair plays a critical role in Zn^{2+} coordination and cleavage activity. Circular dichroism studies indicate that the Rh−P4 conjugate does not coordinate Zn^{2+} in the same manner as the Rh−P1, Rh−P2, Rh−P3, and Rh−P5 conjugates. The Rh−P4 conjugate also cleaves plasmid significantly less efficiently than the Rh−P1 conjugate. Histidine has a larger stability constant than glutamic acid for Zn^{2+} coordination (*46*), and in the P4 peptide, it appears that the glutamic acid residues are not well positioned for effective coordination and delivery of Zn^{2+} to the DNA backbone.

This mutation strategy also allowed us to assess the importance of the glutamic acid in position 4. This residue was originally designed to participate in the hydrolysis reaction by acting as a coordinating ligand, a hydrogen bond acceptor with His, or as a general base catalyst. We examined the function of this Glu residue by replacing it with Ala (Rh−P5 conjugate), by shifting it to the C-terminal side of the peptide (Rh−P2 and Rh−P3 conjugates), and by replacing it with glutamic acid analogues with longer carbon chains and extended reach (Rh−P6 and Rh−P7 conjugates). While the histidine residues were found to be critical for efficient DNA cleavage, this nearby glutamate was found not to be a source of enhancement. All of the conjugates with changes in glutamic acid position within the peptide (Rh−P2, Rh−P3, and Rh−P5 conjugates) display rate constants that closely match the rate constant of the Rh−P1 conjugate. Glutamic acid analogues that extend the reach of the acid functionality group (Rh−P6 and Rh−P7 conjugates) also do not show increased activity relative to the Rh−P1 conjugate. Thus, in the synthetic conjugate, a mechanism involving general base catalysis assisted by a glutamate side chain appears to be unlikely. Notably, the pH profile for the conjugates also supports this conclusion.

The Rh−Bam Conjugate. While small systematic changes in the peptide allow a clarification of the mechanism, much larger changes provide a test of the overall strategy. In fact, the tethered peptide can be significantly altered without losing the hydrolysis activity of the intercalator−peptide chimera. In the case of the Rh−Bam conjugate, a peptide excerpted from the active site of the *Bam*HI endonuclease was appended to $[Rh(phi)_2bpy']^{3+}$ and successfully applied to the conversion of supercoiled plasmid to nicked product. Our appended peptide (NH_2-*Ala*-**Asp**-Val-Tyr-Lys-Glu-Phe-Ile-Glu-Asn-Ser-Glu-Leu-Lys-Arg-Val-Gly-*Ala*-**Glu**-Phe-**Glu**-*Ala*-COOH) is 22 amino acids long and contains the three acidic residues (shown in bold) that are essential to *Bam*HI cleavage activity. Only very slight changes in the hairpin sequence were made prior to appending the peptide; an alanine residue was added to the N-terminus of the peptide to give flexibility to the peptide−DNA interaction, and methio-

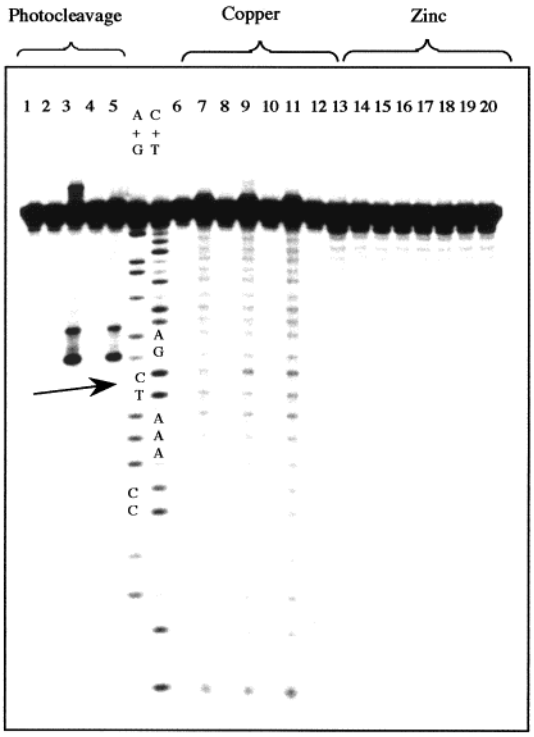

FIGURE 11: Rh−chrysi−P1 photocleavage, Zn^{2+} cleavage, and Cu^{2+} cleavage of a 25-mer oligonucleotide substrate with a CC mismatch. The arrow denotes the position of the CC mismatch Photocleavage: lane 1, light control, irradiation without the rhodium complex; lane 2, Rh[(phen)(bpy′′)(chrysi)]$^{3+}$, no irradiation; lane 3, irradiation with Rh[(phen)(bpy′′)(chrysi)]$^{3+}$; lane 4, Rh−chrysi−P1 conjugate, no irradiation; and lane 5, irradiation with the Rh−chrysi−P1 conjugate. Copper cleavage: lane 6, DNA in Tris buffer; lane 7, Cu^{2+} with MPA; lane 8, Rh[(phen)(bpy′′)(chrysi)]$^{3+}$; lane 9, Rh[(phen)(bpy′′)(chrysi)]$^{3+}$ with Cu^{2+} and MPA; lane 10, Rh−chrysi−P1 conjugate; lane 11, Rh−chrysi−P1 conjugate with Cu^{2+} and MPA; and lane 12, Rh−chrysi−P1 conjugate with Cu^{2+}. Zinc cleavage: lane 13, DNA in buffer; lane 14, 50 μM Zn^{2+}; lane 15, Rh[(phen)(bpy ′′)(chrysi)]$^{3+}$; lane 16, Rh[(phen)(bpy′′)(chrysi)]$^{3+}$ with 5 μM Zn^{2+}; lane 17, Rh[(phen)(bpy′′)(chrysi)]$^{3+}$ with 50 μM Zn^{2+}; lane 18, Rh−chrysi−P1 conjugate; lane 19, Rh−chrysi−P1 conjugate with 5 μM Zn^{2+}; and lane 20, Rh−chrysi−P1 conjugate with 50 μM Zn^{2+}.

nine and threonine residues were replaced with alanine residues to simplify the synthesis and reactivity of the peptide.

The conformations of the free peptide and the tethered peptide were probed by circular dichroism spectroscopy, but it is still not clear whether the 22-mer retains any of its native conformation outside of the *Bam*HI environment. The CD spectra observed for β turns and hairpins are weak and highly variable compared to the spectra for α helices (*47*), so the absence of striking features in the CD spectra does not rule out a β hairpin population. Notably, the peptide contains a total of six glutamic acid residues, and it is possible that any of these residues might be involved in zinc coordination and delivery, particularly if the peptide is not folding into a hairpin conformation.

The Rh−Bam conjugate effectively cleaves supercoiled plasmid, but unlike the Rh−P1 conjugate, it does not generally produce linear plasmid and has not yet been demonstrated to cleave DNA oligonucleotides. It is noteworthy that many of the artificial nucleases in the literature have only been reported to cleave supercoiled DNA, and have not been demonstrated to cleave linear substrates. The plasmid cleavage assay is at least 1 order of magnitude more sensitive than the cleavage assay with an oligonucleotide (*40*), and in some cases, the weak activity of the reagent may be the source of the difficulty. However, this difference in assay sensitivity does not appear to account for the lack of reaction of the Rh−Bam conjugate on oligonucleotides. Additionally, the strain inherent in a supercoiled plasmid or a few damaged sites in a 3 kb plasmid may be an important factor in activating DNA for hydrolysis (*48*). The failure of the Rh−Bam conjugate to produce linear DNA in the plasmid cleavage assay is notable in this context. Intercalation could be considered a source of strain energy, which perhaps the conjugate containing the shorter P1 peptide exploits more effectively than the Rh−Bam conjugate.

Because the Rh−Bam conjugate has not been demonstrated to cleave oligonucleotides, it has not been possible to analyze directly the cleavage products and thus establish the hydrolytic chemistry. Nonetheless, the requirement for redox-inactive Zn^{2+} in Rh−Bam cleavage assays and the similarity in other reaction characteristics to the Rh−P1 conjugate point to hydrolysis as the probable mechanism.

The Divalent Metal Cation. There is now considerable appreciation for the catalytic and structural roles that Zn^{2+} plays in proteins and enzymes (*49*); indeed, hundreds of proteins with Zn^{2+} centers have been identified and characterized. Under physiological conditions, zinc exists as a divalent cation. The d shell of Zn^{2+} is completely filled, and this has several important consequences. Zn^{2+} tolerates a variety of coordination geometries, is relatively labile, is not redox-active, and is spectroscopically silent. Catalytic zinc centers usually have distorted tetrahedral geometry and commonly involve histidine and solvent coordination (*50*). Zn^{2+} very effectively promotes the nucleophilicity of bound water, in some instances lowering the pK_a of water from ~16 to 7 (*51*).

All of these characteristics make Zn^{2+} a very promising candidate metal ion for an artificial nuclease. In particular, the flexible coordination geometry and the low coordination number of Zn^{2+} are well suited for coordination by a short peptide. After consideration of the active sites of several hydrolytic metalloenzymes, the P1 peptide was designed with a coordination site for Zn^{2+} consisting of two histidine residues at the i and $i + 4$ positions in the peptide. This His−Zn^{2+}−His motif has been observed in naturally occurring and designed helices (*43*, *52*). The Bam peptide does not contain any histidine residues, the most common Zn^{2+} ligand in catalytic sites, but because Zn^{2+} is a borderline hard−soft Lewis acid, glutamate and aspartate residues can also serve as coordinating ligands.

Interestingly, the helicity and activity of the Rh−P1 conjugate are both very sensitive to Zn^{2+} concentration, and maximum helicity and activity both occur with stoichiometric amounts of zinc ion. These results are consistent with the coordination model in which His7 and His11 bind the zinc ion on one turn of the α helix (*40*). Presumably as a greater than stoichiometric Zn^{2+} concentration is added, the His residues begin to separately coordinate zinc, and no longer nucleate helix formation. The interesting correlation between helical content and activity suggests that the conformation of the peptide is important in the activation of DNA for hydrolysis. The Rh−Bam peptide exhibits behavior very different from that of the Rh−P1 conjugate when titrated

with Zn^{2+}. The observation that cleavage activity is maintained as the Zn^{2+} concentration is increased significantly above stoichiometric levels suggests that Zn^{2+} is not playing a critical role in nucleating formation of an active conformation.

For both the Rh−P1 family of conjugates and the Rh−Bam conjugate, the level of DNA cleavage decreases as the pH is increased above pH 6. The reason for the sensitivity of the reaction to pH is likely, at least in part, the result of decreased solubility of Zn^{2+} at higher pH. It appears that the coordination environment created by the Rh−P1 or Rh−Bam conjugate is insufficient to prevent Zn^{2+} precipitation. This issue of solubility has made it very difficult to control the hydrolysis of DNA by our metal−peptide conjugate.

Zn^{2+} is not the only metal ion that can be effectively delivered to DNA by the Rh−P1 and Rh−Bam conjugates. Cadmium ion can be substituted for zinc ion with some loss of cleavage activity. Cd^{2+} also has a filled d shell, but it is a much softer metal with a larger radius and greater polarizability (*50*). The Rh−Bam conjugate, which includes acidic residues that should be particularly effective for coordinating hard ions, can also promote a modest amount of cleavage with Mg^{2+}. Magnesium is the ion used by most restriction enzymes, including *Bam*HI, in DNA hydrolysis. Mg^{2+} is redox inert, has a high charge density, boasts a coordination number of 6, and prefers hard oxoanion ligands. Mg^{2+} is extensively hydrated, preferring water over bulkier ligands, but it does not activate water for nucleophilic attack to the same extent as Zn^{2+} (*53*). Zn^{2+} gives higher percentages of nicked plasmid than Mg^{2+} when incubated with the Rh−Bam conjugate and supercoiled plasmid, and this is not surprising given the properties of these two important biological metal ions. The Rh−P1 conjugate is not able to hydrolyze plasmid in the presence of Mg^{2+}, presumably because histidine is not an effective ligand for hard cations such as Mg^{2+}.

Two redox-active metals, Fe^{2+} and Cu^{2+}, have also been tested with our metallointercalator−peptide conjugates. Combining the Rh−P1 conjugate and Fe^{2+} with plasmid resulted in 80% nicked plasmid. This activity is considerable, but it still does not match the results achieved with Zn^{2+}. In plasmid cleavage assays, Cu^{2+}, without the rhodium complex, promotes considerable formation of nicked plasmid even at 5 μM. Interestingly, the addition of the Rh−P1 or Rh−Bam conjugate actually caused a decrease in the percentage of nicked plasmid generated by Cu^{2+}. Apparently, the conjugates provide modest protection for the plasmid, perhaps by sequestering some of the copper or by blocking access to the DNA backbone. In cleavage experiments with restriction fragments from the pUC19 plasmid, 20 μM Cu^{2+} did not produce any observable damage to the DNA. The addition of a reducing agent to effect catalytic turnover resulted in very modest cleavage distributed evenly over the length of the fragment. The addition of the Rh−P1 conjugate and MPA resulted in intense cleavage at selected sites in the fragment. These results again emphasize the differences between supercoiled plasmid and linear DNA cleavage assays.

The copper cleavage experiments with restriction fragments and the Rh−P1 conjugate revealed some of the requirements for metallointercalator−peptide interactions with DNA. Comparisons of photocleavage and copper cleavage patterns demonstrated that binding of the metallointercalator in and of itself is not sufficient for promoting copper cleavage. Photocleavage results revealed that the metallointercalator−peptide conjugate binds across the restriction fragment with only a slight preference for ACG sites. In contrast, Rh−P1-promoted copper cleavage occurred intensely at very few sites. To achieve oxidative strand scission, then, not only must the metallointercalator bind to the DNA, but the flexible P1 peptide must also be correctly oriented to deliver copper to the backbone. With a short peptide like the Rh−AHAAHA conjugate, the correct orientation for copper delivery is more accessible. The slight preference for copper cleavage at AT-rich sequences for both the Rh−AHAAHA and Rh−P1 conjugates suggests that the flexibility of the DNA may also be important for reaction.

Neither the P1 nor the AHAAHA peptide is optimized for copper binding, yet they do promote copper cleavage of the DNA backbone. With an optimized copper binding motif, such as Gly-Gly-His (*54*, *55*), an intercalator−peptide conjugate might be a very interesting tool for promoting oxidative copper damage to DNA.

The Metallointercalator. Intercalators are very useful for the delivery of small peptides to DNA and RNA (*56*−*58*), and several groups have successfully applied intercalators to the design of artificial nucleases. For example, an active tetrapeptide was attached to an acridine intercalator, and the histidine residues were found to promote RNA cleavage (*59*, *60*). More recently, using a strategy very similar to our own, a peptide with unnatural zinc-coordinating residues was delivered to DNA by conjugation with acridine (*15*).

In our group, much effort has been invested in the synthesis and characterization of DNA−intercalating metal complexes (*61*). Such complexes have proven to be useful as tools for probing DNA recognition (*62*) and DNA-mediated electron transfer chemistry (*63*). We have also developed general methods for coupling peptides to metallointercalators for achieving both interesting DNA recognition (*39*, *56*, *57*) and now reactivity (*25*).

Our detailed biochemical and structural studies of sequence-specific metallointercalators provide us with a valuable foothold as we seek to design a restriction enzyme mimic (*31*−*33*, *56*, *57*, *64*, *65*). A true artificial restriction enzyme would selectively hydrolyze a specific sequence in a DNA duplex. Although several laboratories have attached artificial nucleases to oligonucleotides and thus have achieved selective hydrolysis of a complementary RNA or DNA strand (*66*−*70*), effective strategies for targeting duplex DNA have not yet been devised. Harnessing a sequence-specific metallointercalator to deliver a reactive moiety to duplex DNA would be a very effective way of generating sequence-specific hydrolysis.

In our initial design, the sequence-neutral intercalator $[Rh(phi)_2bpy]^{3+}$ was selected for conjugation with our peptide. This particular complex binds with high affinity, and the bipyridine ancillary ligand can be conveniently modified to create a carboxylate arm for peptide coupling. With $[Rh(phi)_2bpy]^{3+}$, we have successfully delivered two very different peptides to the DNA backbone to promote hydrolysis.

The $[Rh(phi)_2bpy]^{3+}$ complex is able to cleave DNA when irradiated at 313 nm, and photocleavage studies suggest that neither the P1 nor the Bam peptide significantly changes the

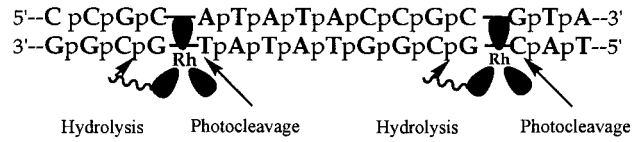

FIGURE 12: Schematic illustration of the relationship between intercalation and hydrolysis of DNA by the Rh−P1 conjugate. [Rh(phi)$_2$bpy′]$^{3+}$ is intercalated in the center of two 5′-Pu-Py-Pu-Py-3′ sites and promotes photoactivated oxidative cleavage at the pyrimidine which is 5′ to the intercalation site. The appended peptide delivers the divalent cation to the 3′ phosphodiester linkage at which hydrolytic cleavage occurs.

DNA recognition properties of this sequence-neutral intercalator. From relative photocleavage intensities, it appears that the peptide may reduce the binding affinity of the complex slightly, but this effect has not been quantified. Interactions between the rhodium complex and the peptide have not been ruled out, but the absorption characteristics of [Rh(phi)$_2$bpy]$^{3+}$ are not perturbed by the attachment of a peptide. Together with the photocleavage levels, this suggests minimal interaction between the ligands and the peptide. The peptides do not contribute DNA recognition characteristics to the intercalator, but neither do they appear to fold around the complex to prevent DNA binding and photocleavage activity. Photocleavage and hydrolysis reactions allow us to map the interactions of the conjugate with DNA. In experiments with a 42-mer duplex, hydrolysis was consistently observed at a phosphodiester linkage on the 3′ side of the intercalation site, and a model consistent with this cleavage pattern is presented in Figure 12.

The intercalator gives our artificial nuclease a critical advantage. By providing DNA binding affinity, the intercalator allows us to hydrolyze DNA with very low artificial nuclease concentrations. The activity of the P1 peptide at a concentration of 5 μM is very modest unless it is tethered to [Rh(phi)$_2$bpy′]$^{3+}$ (Table 1). Of course, it is possible that the rhodium intercalator is more than a passive delivery system. The strain and unwinding that results from DNA intercalation may be a factor in the DNA hydrolysis observed with our conjugates (vide supra).

The P1 peptide has also been tethered to ethidium, an organic DNA intercalator (*71*). In contrast to [Rh(phi)$_2$bpy′]$^{3+}$, ethidium intercalates via the minor groove of DNA, and it would be interesting to compare the regioselectivity of a conjugate delivered from the minor groove to the regioselectivity of the Rh−P1 conjugate. Attachment of the peptide to *N*-8-glycylethidium did not produce an active nuclease; in fact, the ethidium−peptide conjugate appears to form a tridentate chelate of Zn^{2+} that can no longer intercalate into DNA. Visible and CD spectra suggest that the two histidine residues of P1 and one of the exocyclic nitrogen amines of ethidium coordinate to Zn^{2+} (*71*).

Aiming for site-specific hydrolysis, we attached the P1 peptide to [Rh(phen)(bpy″)(chrysi)]$^{3+}$. This three-ligand metallointercalator preferentially binds at DNA sites that are destabilized by mismatches. The [Rh(bpy)$_2$chrysi]$^{3+}$ complex has been demonstrated to bind and photocleave 80% of the possible DNA mismatches (*33*), and it would be interesting to use a chrysi complex to target hydrolysis to mismatch sites. Photocleavage experiments with the Rh−chrysi−P1 conjugate confirmed binding at a CC mismatch site. The peptide caused only a modest decrease in photocleavage intensity relative to [Rh(bpy)$_2$chrysi]$^{3+}$. Although the conjugate is clearly binding at mismatch sites, Zn^{2+}-promoted hydrolysis has not yet been observed, and there was no peptide-dependent Cu^{2+} damage near the mismatch site (Figure 11). With this intercalator and with this sequence of DNA, the P1 peptide is not correctly positioned to promote cleavage of the DNA backbone. This is consistent with our copper cleavage studies with the Rh−P1 conjugate, and again suggests that binding of the metallointercalator does not guarantee corresponding copper damage.

These results with ethidium and the chrysi metallointercalator together suggest that the selection of an intercalator is a critical element in the design of our artificial nucleases. Not all metallointercalators orient a metallopeptide for the initiation of DNA hydrolysis, and it may be necessary to vary linkers and ancillary ligands to optimize activity. The selection of [Rh(phi)$_2$bpy′]$^{3+}$ as the metallointercalator for our first generation of artificial nucleases was an opportune choice, for we were able to achieve reactivity without manipulation of the linker or ligands.

CONCLUSION

This general strategy of appending metal-coordinating functionality, indeed even peptide architectures, to metallointercalators provides a new approach to the hydrolysis of the phosphodiester backbone of DNA. While the metal−peptide structures and their orientations on the DNA helix require better definition and control, such designed nucleases boast several attractive features to provide a foundation for a new generation of metal-based tools for targeting and manipulating DNA.

ACKNOWLEDGMENT

We are grateful to Dr. Ulrike Riese for synthesis of the bpy″ ligand and to the Biopolymer Synthesis Facility at the California Institute of Technology for preparation of peptides.

REFERENCES

1. Williams, N. H., Takasaki, B., Wall, M., and Chin, J. (1999) *Acc. Chem. Res. 32*, 485−493.
2. Westheimer, F. H. (1987) *Science 235*, 1173−1178.
3. Eigner, J., Boedtker, H., and Michaels, G. (1961) *Biochim. Biophys. Acta 51*, 165−168.
4. Linn, S. M., Llyod, R. S., and Roberts, R. J. (1993) *Nucleases*, Cold Spring Harbor Laboratory Press, Plainview, NY.
5. Hegg, E. L., and Burstyn, J. N. (1998) *Coord. Chem. Rev. 173*, 133−165.
6. Sigman, D. S., Mazumder, A., and Perrin, D. M. (1993) *Chem. Rev. 93*, 2295−2316.
7. Dervan, P. B. (1986) *Science 232*, 464−471.
8. Meunier, B. (1992) *Chem. Rev. 92*, 1411−1456.
9. Sreedhara, A., and Cowan, J. A. (2001) *J. Biol. Inorg. Chem. 6*, 337−347.
10. Dixon, N., Geue, R., Lambert, J., Moghaddas, S., Pearce, D., and Sargeson, A. (1996) *Chem. Commun.*, 1287−1288.
11. Hettich, R., and Schneider, H. (1997) *J. Am. Chem. Soc. 119*, 5638−5647.
12. Hegg, E., and Burstyn, J. (1995) *Inorg. Chem. 34*, 7474−7481.
13. Ren, R., Yang, P., Zheng, W., and Hua, Z. (2000) *Inorg. Chem. 39*, 5454−5463.
14. Itoh, T., Hisada, H., Sumiya, T., Hosono, M., Usui, Y., and Fujii, Y. (1997) *J. Chem. Soc., Chem. Commun.*, 677−678.

15. Sissi, C., Rossi, P., Felluga, F., Formaggio, F., Palumbo, M., Tecilla, P., Toniolo, C., and Scrimin, P. (2001) *J. Am. Chem. Soc. 123*, 3169−3170.
16. Aka, F. N., Akkaya, M. S., and Akkaya, E. U. (2001) *J. Mol. Catal. A: Chem. 165*, 291−294.
17. Ragunathan, K. G., and Schneider, H. (1996) *Angew. Chem., Int. Ed. Engl. 35*, 1219−1221.
18. Roigk, A., Hettich, R., and Schneider, H. (1998) *Inorg. Chem. 37*, 751−756.
19. Hashimoto, S., and Nakamura, Y. (1996) *J. Chem. Soc., Perkin Trans. 1*, 2623−2627.
20. Takasaki, B., and Chin, J. (1994) *J. Am. Chem. Soc. 116*, 1121−1122.
21. Komiyama, M., Takeda, N., Takahashi, Y., Uchida, H., Shiiba, T., Kodama, T., and Yashiro, M. (1995) *J. Chem. Soc., Perkin Trans. 2*, 269−274.
22. Komiyama, M., and Sumaoka, J. (1998) *Curr. Opin. Chem. Biol. 2*, 751−757.
23. Branum, M. E., Tipton, A. K., Zhu, S., and Que, L., Jr. (2001) *J. Am. Chem. Soc. 123*, 1898−1904.
24. Sreedhara, A., Freed, J. D., and Cowan, J. A. (2000) *J. Am. Chem. Soc. 122*, 8814−8824.
25. Fitzsimons, M., and Barton, J. K. (1997) *J. Am. Chem. Soc. 119*, 3379−3380.
26. Pyle, A., Long, E., and Barton, J. K. (1989) *J. Am. Chem. Soc. 111*, 4520−4522.
27. Sitlani, A., Long, E. C., Pyle, A. M., and Barton, J. K. (1992) *J. Am. Chem. Soc. 114*, 2303−2312.
28. Sitlani, A., and Barton, J. K. (1994) *Biochemistry 33*, 12100−12108.
29. Newman, M., Straelecka, T., Dorner, L. F., Schildkraut, I., and Aggarwal, A. K. (1995) *Science 269*, 656−663.
30. Viadiu, H., and Aggarwal, A. K. (1998) *Nat. Struct. Biol. 5*, 910−916.
31. Jackson, B. A., and Barton, J. K. (1997) *J. Am. Chem. Soc. 119*, 12986−12987.
32. Jackson, B. A., Alekseyev, V. Y., and Barton, J. K. (1999) *Biochemistry 38*, 4655−4662.
33. Jackson, B. A., and Barton, J. K. (2000) *Biochemistry 39*, 6176−6182.
34. Ciana, L. D., Hamachi, I., and Meyer, T. J. (1989) *J. Org. Chem. 54*, 1731−1735.
35. Gillard, R. D., Osborn, J. A., and Wilkinson, G. J. (1965) *J. Chem. Soc.*, 1951−1965.
36. Pyle, A. M., Chiang, M. Y., and Barton, J. K. (1990) *Inorg. Chem. 29*, 4487−4495.
37. Jones, R. C. F., and Schofield, J. (1990) *J. Chem. Soc., Perkin Trans. 1*, 375−383.
38. Murner, H., Jackson, B. A., and Barton, J. K. (1998) *Inorg. Chem. 37*, 3007.
39. Sardesai, N. Y., Lin, S. C., Zimmermann, K., and Barton, J. K. (1995) *Bioconjugate Chem. 6*, 302−312.
40. Fitzsimons, M. P. (1998) Ph.D. Thesis, California Institute of Technology, Pasadena, CA.
41. Lehrman, S. R., Tuls, J. L., and Lund, M. (1990) *Biochemistry 29*, 5590−5596.
42. Pyle, A. M. (1989) Ph.D. Thesis, Columbia University, New York.
43. Ghadiri, M. R., and Choi, C. (1990) *J. Am. Chem. Soc. 112*, 1630−1632.
44. Hastings, C. A., and Barton, J. K. (1999) *Biochemistry 38*, 10042−10051.
45. DeGrado, W. (1999) *Annu. Rev. Biochem. 68*, 779−819.
46. Perrin, D. D. (1979) *Organic Ligands*, pp 412−416, Pergamon Press, Oxford, U.K.
47. Perczel, A., and Hollósi, M. (1996) in *Circular Dichroism and the Conformational Analysis of Biomolecules* (Fasman, G. D., Ed.) pp 285−380, Plenum Press, New York.
48. Bashkin, J. K. (1999) *Curr. Opin. Chem. Biol. 3*, 752−758.
49. Berg, J. M., and Shi, Y. (1996) *Science 271*, 1081−1085.
50. Christianson, D. W. (1991) *Adv. Protein Chem. 42*, 281−355.
51. Groves, J. T., and Baron, L. A. (1989) *J. Am. Chem. Soc. 111*, 5442−5448.
52. Matthews, B. W. (1988) *Acc. Chem. Res. 21*, 333−340.
53. Cowan, J. A. (1998) *Chem. Rev. 98*, 1067−1087.
54. Mack, D. P., and Dervan, P. B. (1992) *Biochemistry 31*, 9399−9405.
55. Long, E. C. (1999) *Acc. Chem. Res. 32*, 827−836.
56. Sardesai, N. Y., Zimmermann, K., and Barton, J. K. (1994) *J. Am. Chem. Soc. 116*, 7502−7508.
57. Sardesai, N. Y., and Barton, J. K. (1997) *J. Biol. Inorg. Chem. 2*, 762−771.
58. Tabor, A. B. (1996) *Tetrahedron 52*, 2229−2234.
59. Tung, C., Wei, Z., Leibowitz, M. J., and Stein, S. (1992) *Proc. Natl. Acad. Sci. U.S.A. 89*, 7114−7118.
60. Tung, C., Ebright, Y., Shen, X., and Stein, S. (1992) *Bioorg. Med. Chem. Lett. 2*, 303−306.
61. Erkkila, K. E., Odom, D. T., and Barton, J. K. (1999) *Chem. Rev. 99*, 2777.
62. Johann, T. W., and Barton, J. K. (1996) *Philos. Trans. R. Soc. London, Ser. A 354*, 299−324.
63. Núñez, M. E., and Barton, J. K. (2000) *Curr. Opin. Chem. Biol. 4*, 199−206.
64. Hudson, B. P., and Barton, J. K. (1998) *J. Am. Chem. Soc. 120*, 6877−6888.
65. Kielkopf, C. L., Erkkila, K. E., Hudson, B. P., Barton, J. K., and Rees, D. C. (2000) *Nat. Struct. Biol. 7*, 117−121.
66. Bashkin, J. K., Gard, J. K., and Modak, A. S. (1990) *J. Org. Chem. 55*, 5125.
67. Matsumura, K., Endo, M., and Komiyama, M. (1994) *J. Chem. Soc., Chem. Commun.*, 2019−2020.
68. Hovinen, J., Guzaev, A., Azhayeva, E., Azhayev, A., and Lönnberg, H. (1995) *J. Org. Chem. 60*, 2293−2294.
69. Hall, J., Huesken, D., and Haener, R. (1996) *Nucleic Acids Res. 24*, 3522−3526.
70. Magda, D., Crofts, S., Lin, A., Miles, D., Wright, M., and Sessler, J. L. (1997) *J. Am. Chem. Soc. 119*, 2293−2294.
71. Houser, R. P., Fitzsimons, M. P., and Barton, J. K. (1999) *Inorg. Chem. 38*, 1368−1370.

BI011793K